

Double parton distributions of the proton from basis light-front quantization

Tian-Cai Peng,^{1, 2, 3, 4,*} Zhi Hu,^{5,†} Sreeraj Nair,^{6, 7, 8,‡} Siqi Xu,^{6, 7, 8,§} Xiang Liu,^{1, 2, 3, 4, 9,¶}

Chandan Mondal,^{6, 7, 8,**} Xingbo Zhao,^{6, 7, 8, 10,††} and James P. Vary^{11, ‡‡}

(BLFQ Collaboration)

¹*School of Physical Science and Technology, Lanzhou University, Lanzhou 730000, China*

²*Lanzhou Center for Theoretical Physics, Key Laboratory of Theoretical*

Physics of Gansu Province, Lanzhou University, Lanzhou 730000, China

³*Key Laboratory of Quantum Theory and Applications of MoE, Lanzhou University, Lanzhou 730000, China*

⁴*Research Center for Hadron and CSR Physics, Lanzhou University*

and Institute of Modern Physics of CAS, Lanzhou 730000, China

⁵*High Energy Accelerator Research Organization (KEK), Ibaraki 305-0801, Japan*

⁶*Institute of Modern Physics, Chinese Academy of Sciences, Lanzhou 730000, China*

⁷*School of Nuclear Science and Technology, University of Chinese Academy of Sciences, Beijing 100049, China*

⁸*CAS Key Laboratory of High Precision Nuclear Spectroscopy,*

Institute of Modern Physics, Chinese Academy of Sciences, Lanzhou 730000, China

⁹*MoE Frontiers Science Center for Rare Isotopes, Lanzhou University, Lanzhou 730000, China*

¹⁰*Advanced Energy Science and Technology Guangdong Laboratory, Huizhou, Guangdong 516000, China*

¹¹*Department of Physics and Astronomy, Iowa State University, Ames, IA 50011, U.S.A.*

(Dated: July 11, 2025)

Within the basis light-front quantization framework, we systematically investigate the unpolarized and longitudinally polarized double parton distributions (DPDs) of quarks inside the proton. We utilize the light-front wave functions of the proton derived in the valence sector from a Hamiltonian quantized on the light-front. The interaction terms of the Hamiltonian consist of a one-gluon exchange interaction at fixed coupling and a three-dimensional confinement potential. Our current analysis yields significant correlations of the quarks' longitudinal momenta with their transverse separation. We also demonstrate that our calculations do not support the commonly used $x - \vec{k}_\perp$ factorization of the DPDs in x and \vec{k}_\perp . Our results are qualitatively consistent with those of other phenomenological models.

I. INTRODUCTION

The parton distribution functions (PDFs) are essential for describing the nonperturbative structure of hadrons in high-energy collider measurements, such as those conducted at the Large Hadron Collider (LHC). The PDFs give the probability of finding a parton carrying a certain momentum fraction x inside the hadron probed by single parton scattering [1]. In general, within the same hadron-hadron collision, there is the possibility for multiple hard scattering events and in fact, the contributions from such multiparton interactions (MPIs) [2] increases with increasing energy. The most important and the simplest of these MPIs is double parton scattering (DPS), wherein two partons in each hadron participate in two distinct hard scattering processes. These DPS cross-sections can be parametrized in terms of the nonperturbative distributions called the double parton distributions (DPDs), which effectively quantify the joint probability of finding

the two struck partons with longitudinal momentum fraction x_1 and x_2 , and separated by a transverse distance \vec{y}_\perp inside the hadron. Most DPS studies assume that there is no correlation between the transverse separation and the longitudinal momentum fractions [3–10]. A complete factorization of all the arguments leads to the so-called “pocket formula” [11], wherein the DPS cross section is written as the product of two single parton cross-sections.

The validity of the factorization hypothesis will be examined here through analysis of di-quark correlations in a light-front Hamiltonian framework. We note that the DPDs depend not only on the longitudinal momentum fraction and the transverse separation but they also depend on the renormalization scales μ_1 and μ_2 corresponding to the two struck partons. They obey the QCD evolution equation [12–18] similar to the Dokshitzer-Gribov-Lipatov-Altarelli-Parisi (DGLAP) evolution equations for the PDFs. The evolution of DPDs generally neglects the color correlation [19] between the two partons based on the fact that they are Sudakov suppressed [20, 21] and instead, the color of each individual parton is summed over. Meanwhile, the color-correlated evolution kernel of the DPDs at the next-to-leading order in the strong coupling has been computed in Ref. [22].

Experimentally, DPS events have been observed at the Tevatron and the LHC for a wide range of final states [5, 7, 23–26] with future LHC data expected to yield better insights. In upcoming electron-ion collision

* pengtc20@lzu.edu.cn

† huzhi0826@gmail.com; *Corresponding author

‡ sreeraj@impcas.ac.cn

§ xsq234@impcas.ac.cn

¶ xiangliu@lzu.edu.cn

** mondal@impcas.ac.cn

†† xbzhao@impcas.ac.cn

‡‡ jvary@iastate.edu

experiments [27, 28], it may also be feasible to measure DPDs by examining the interaction between two photons and the nucleon [29–31].

The foundational theory on DPS was laid several decades ago providing remarkable insights [32–34]. Several studies have been performed in the last decade to improve our theoretical understanding of DPS [21, 35–41]. The DPDs are constrained by sum rules based on quark number and conservation of momentum [42–45] and also from their nature in the limit of small distances between the two struck partons [46, 47]. Several studies exist on DPDs in QCD-inspired models [48–61]. The DPS is also considered for physics beyond the Standard Model [62] as well as in the background of precision studies [63]. A few of the recent investigations both from theory and phenomenology can be found in Refs. [64–70]. Additionally, Euclidean lattice QCD stands out as a promising theoretical framework for calculating DPDs of the nucleon [71–73].

In this work, we adopt the basis light-front quantization (BLFQ) approach [74], a recently developed non-perturbative framework, to calculate the DPDs of the proton. With the framework of BLFQ, the light-front wave functions (LFWFs) of a bound state are obtained by diagonalizing the light-front Hamiltonian in a truncated Fock space [75]. The BLFQ approach has been successfully employed in QED systems [76–82] as well as in several QCD bound systems [83–105]. Recent studies within BLFQ that go beyond the valence Fock sector, thereby incorporating gluon dynamics, can be found in Refs. [104–108]. Here, we adopt a light-front effective Hamiltonian for the proton in the constituent valence quark Fock space ($|qqq\rangle$) and solve for its mass eigenstates and LFWFs. Parameters in this Hamiltonian have been fitted to generate the proton mass and the electromagnetic properties of the nucleon [95, 96]. The resulting LFWFs have successfully been used to investigate various proton properties, such as electromagnetic and axial form factors, radii, PDFs, GPDs, TMDs, and angular momentum distributions, etc., [95–98, 100, 103]. Here, we extend those investigations to study both the unpolarized and longitudinally polarized quark DPDs of the proton.

We structure the paper as follows. Section II introduces the BLFQ framework and outlines our Hamiltonian, which we diagonalize to derive the LFWFs. In section III, we present the overlap representation for both unpolarized and polarized DPDs. Section IV presents our numerical results obtained using the resulting LFWFs. Finally, we present our summary and outlooks in section V.

II. BASIS LIGHT-FRONT QUANTIZATION

In BLFQ, we aim to solve the light-front eigenvalue problem, expressed as: $H_{\text{LC}}|\psi_h\rangle = M_h^2|\psi_h\rangle$, where the light-front Hamiltonian, $H_{\text{LC}} = (P^+P^- - P_\perp^2)$, incor-

porates the longitudinal momentum¹ P^+ , the light-front energy P^- , and the transverse momentum \vec{P}_\perp . Solving this equation with a suitable matrix representation for H_{LC} yields the invariant-mass spectrum M_h and light-front state vectors $|\psi_h\rangle$, which provide the LFWFs when expanded in momentum space.

The expansion of the state $|\psi_h\rangle$ within one Fock sector utilizes a complete set of orthonormal basis states. The BLFQ basis comprises transverse two-dimensional (2D) harmonic-oscillator (HO) modes, discretized longitudinal plane waves, and the light-front helicity eigenstates. Thus, basis states are characterized by four quantum numbers $\alpha = (k, n, m, s)$, where n and m are the principal and orbital angular quantum numbers in the transverse plane, respectively, s denotes the light-front helicity, and k represents the longitudinal momentum.

The orthonormalized 2D-HO basis functions in momentum space are expressed as [74, 110]:

$$\phi_{n,m}(\vec{k}_\perp; b) = \frac{\sqrt{2}}{b(2\pi)^{\frac{3}{2}}} \sqrt{\frac{n!}{(n + |m|)!}} e^{-\vec{k}_\perp^2/(2b^2)} \times \left(\frac{|\vec{k}_\perp|}{b}\right)^{|m|} L_n^{|m|} \left(\frac{\vec{k}_\perp^2}{b^2}\right) e^{im\theta}, \quad (1)$$

with b as the HO basis scale parameter, and L_n^m the generalized Laguerre polynomials. To obtain a finite basis as a requirement from numerical calculations, we further implement the following truncation in the transverse plane $\sum_i (2n_i + |m_i| + 1) \leq N_{\max}$, where N_{\max} is the total number of oscillator quanta above the minimum required by the Pauli principle.

Longitudinal modes are discretized by imposing periodic or antiperiodic boundary conditions for bosons and fermions, respectively, within a box of length $2L$, leading to the discretized plane wave in coordinate space: $\psi_k(x^-) = \frac{1}{2L} e^{i\frac{\pi}{L} k x^-}$, with quantum number k as integer (bosons) or half-integer (fermions). Total longitudinal momentum P^+ is conserved for all basis states with $P^+ = \pi K/L$ and the longitudinal momentum fraction is $x_i \equiv p_i^+/P^+ = k_i/K$.

Due to the use of the single-particle basis, the solved eigenstates also contain the center-of-mass (CM) motion. To avoid the contamination of the CM motion, a Lagrange multiplier is added to adjust the Hamiltonian: $H' = H_{\text{LC}} + \lambda_L(H_{\text{CM}} - 2b^2 I)$, where the CM motion is governed by a HO potential [78]: $H_{\text{CM}} = \left(\sum_i \vec{k}_{i\perp}\right)^2 + b^4 \left(\sum_i x_i \vec{r}_{i\perp}\right)^2$. The introduction of the Lagrange multiplier, together with the use of the HO basis and the N_{\max} truncation allows for the factorization of the CM and intrinsic components of the LFWFs.

¹ We adopt a convention for the light-front variables [109] such that for a given four-vector x^μ , we have $x^\pm = x^0 \pm x^3$ and the remaining transverse degrees of freedom are denoted by $\vec{x}_\perp = (x_1, x_2)$.

This study focuses exclusively on the leading Fock sector to set an initial baseline for the valence quark contributions. With this Fock truncation, we introduce an effective light-front Hamiltonian given by

$$H_{\text{eff}} = \sum_i \frac{\vec{k}_{i\perp}^2 + m_i^2}{x_i} + \frac{1}{2} \sum_{i,j} V_{ij}^{(\text{CON})} + \frac{1}{2} \sum_{i,j} V_{ij}^{(\text{OGE})}, \quad (2)$$

as an initial model for the first-principles H_{LC} appropriate to the Fock sector truncation. In the effective light-front Hamiltonian H_{eff} , the conditions $\sum_i x_i = 1$ and $\sum_i \vec{k}_{i\perp} = \vec{P}_\perp$ are enforced for momentum conservations, m_i represents the constituent mass of the quark, and indices i and j identify different partons within the Fock sector. The first component of the Hamiltonian is the kinetic energy. The second and third terms are the confinement potential (CON) and the one-gluon exchange interaction (OGE) respectively.

The confinement potentials are designed to act in both transverse and longitudinal directions. Specifically, the transverse confinement potential draws inspiration from the soft-wall (SW) holographic model [111], which is extended to a many-body framework as,

$$V_{ij}^{\text{SW}} = \kappa^4 x_i x_j (\vec{r}_{i\perp} - \vec{r}_{j\perp})^2. \quad (3)$$

For the longitudinal confinement potential [89], the many-body generalized form can be written as follows:

$$V_{i,j}^{\text{L}} = \frac{\kappa^4}{(m_i + m_j)^2} \partial_{x_i} (x_i x_j \partial_{x_j}). \quad (4)$$

The strength of the confining potential is represented by the parameter κ . Consequently, the complete confinement potential is expressed as $V_{ij}^{(\text{CON})} = V_{ij}^{\text{SW}} + V_{ij}^{\text{L}}$.

The OGE interaction is expressed as,

$$V_{ij}^{\text{OGE}} = \frac{4\pi\alpha_s C_F}{Q_{ij}^2} \bar{u}_{s'_i}(k'_i) \gamma^\mu u_{s_i}(k_i) \bar{u}_{s'_j}(k'_j) \gamma_\mu u_{s_j}(k_j). \quad (5)$$

Here $Q_{ij}^2 = -(1/2)(k'_i - k_i)^2 - (1/2)(k'_j - k_j)^2$ represents the squared average momentum transfer, where $k_i(k'_i)$ and $k_j(k'_j)$ are the initial (final) momenta of particles i and j , respectively. $u_{s_i}(k_i)$ denotes the Dirac spinor for a particle with momentum k_i and spin s_i . The α_s indicates the strength of the OGE interaction. The negative value of color factor $C_F = -2/3$ signifies that the OGE potential is attractive.

Diagonalizing the above light-front Hamiltonian using the BLFQ basis yields eigenvalues that define the mass spectrum, together with the associated eigenvectors that describe the inner structures of the systems. The lowest mass eigenstate is identified as the proton state. The proton state with momentum P and helicity Λ within the valence Fock sector can be expressed using three-particle LFWFs as,

$$|P, \Lambda\rangle = \int [d\mathcal{X} d\mathcal{P}_\perp]$$

$$\times \Psi_{\{x_i, \vec{k}_{i\perp}, s_i\}}^\Lambda \left| \left\{ x_i P^+, \vec{k}_{i\perp} + x_i \vec{P}_\perp, s_i \right\} \right\rangle, \quad (6)$$

where the shorthand notation used for the integration measure is written as,

$$\begin{aligned} [d\mathcal{X} d\mathcal{P}_\perp] &= \prod_{i=1}^3 \left[\frac{dx_i d^2 \vec{k}_{i\perp}}{16\pi^3} \right] \\ &\times 16\pi^3 \delta \left(1 - \sum_{i=1}^3 x_i \right) \delta^2 \left(\sum_{i=1}^3 \vec{P}_\perp - \vec{k}_{i\perp} \right). \end{aligned} \quad (7)$$

The LFWFs are expressed in terms of the basis functions as:

$$\begin{aligned} \Psi_{\{x_i, \vec{k}_{i\perp}, s_i\}}^\Lambda &= \sum_{\{k_i, n_i, m_i\}} \psi_{\{k_i, n_i, m_i, s_i\}}^\Lambda \\ &\left(\prod_i \delta_{x_i}^{k_i} \right) \left(\prod_i \phi_{n_i, m_i}(\vec{k}_{i\perp}; b) \right), \end{aligned} \quad (8)$$

where $\psi_{\{k_i, n_i, m_i, s_i\}}^\Lambda = \langle P, \Lambda | \{k_i, n_i, m_i, s_i\} \rangle$ represents the proton's LFWF in the BLFQ basis, obtained from diagonalizing the light-front Hamiltonian. Here, $\phi_{n_i, m_i}(\vec{k}_{i\perp}; b)$ is the orthonormalized 2D harmonic oscillator defined in Eq. 1, and $\delta_{x_i}^{k_i}$ stands for the Kronecker delta.

The parameters within the effective Hamiltonian are tuned to accurately reflect the nucleon mass and its electromagnetic characteristics [96]. The model LFWFs have been utilized to explore a diverse range of nucleon properties, such as electromagnetic and axial form factors, radii, PDFs, quark helicity asymmetries, GPDs, TMDs and angular momentum distributions, etc. [95–98, 100, 103]. These studies have achieved notable success, demonstrating the comprehensive applicability of the current model in calculating hadron observables by solving bound state eigenvalue problems.

III. DOUBLE PARTON DISTRIBUTIONS

The DPDs of a hadron provide a probabilistic framework that describes the likelihood of encountering two partons, each with specified polarization and momentum fractions x_i , situated at a specific relative transverse distance \vec{y}_\perp . The DPDs of quarks in an unpolarized proton are defined by a matrix element involving two operators [39, 46],

$$\begin{aligned} F_{a_1 a_2}(x_1, x_2, y_\perp) &= 2p^+ \int dy^- \int \frac{dz_1^-}{2\pi} \frac{dz_2^-}{2\pi} e^{i(x_1 z_1^- + x_2 z_2^-) p^+} \\ &\times \langle P, \Lambda | \mathcal{O}_{a_1}(y, z_1) \mathcal{O}_{a_2}(0, z_2) | P, \Lambda \rangle. \end{aligned} \quad (9)$$

The operators appearing in Eq. (9) are defined as,

$$\mathcal{O}_a(y, z) = \bar{\psi} \left(y - \frac{z}{2} \right) \Gamma_a \psi \left(y + \frac{z}{2} \right) \Big|_{z^+ = y^+ = 0, \vec{z}_\perp = 0}, \quad (10)$$

where a specifies the polarization of the quark, which is determined by the spin projections through

$$\Gamma_q = \frac{1}{2} \gamma^+, \quad \Gamma_{\Delta_q} = \frac{1}{2} \gamma^+ \gamma_5, \quad \Gamma_{\delta_q}^j = \frac{1}{2} i \sigma^{j+} \gamma_5. \quad (11)$$

Here $j = (1, 2)$ and the notations appearing in the subscript q , Δ_q and δ_q refer to unpolarized, longitudinally polarized, and transversely polarized quark, respectively. We choose the light-cone gauge, and thus the gauge link in this bilocal operator is reduced to unity.

Substituting the proton state Eq. (6) into Eq. (9), from the unpolarized operator corresponding to $\Gamma_q = \frac{1}{2} \gamma^+$, we obtain the following expression for the unpolarized quark DPDs in terms of the overlap of LFWFs,

$$F_{q_1 q_2}(x_1, x_2, \vec{y}_\perp) = \sum_{s_i} \int d^2 \vec{k}_{1\perp} d^2 \vec{k}_{2\perp} d^2 \vec{k}'_{1\perp} \\ \times \Psi_{\{x_i, \vec{k}'_{i\perp}, s_i\}}^{\dagger*} \Psi_{\{x_i, \vec{k}_{i\perp}, s_i\}}^\dagger e^{i(\vec{k}'_{1\perp} - \vec{k}_{1\perp}) \cdot \vec{y}_\perp}, \quad (12)$$

where for struck quarks we have $\vec{k}'_{2\perp} = \vec{k}_{1\perp} + \vec{k}_{2\perp} - \vec{k}'_{1\perp}$ and $\vec{k}'_{3\perp} = \vec{k}_{3\perp} = -(\vec{k}_{1\perp} + \vec{k}_{2\perp})$ for the spectator. x_1 and x_2 are the longitudinal moment fractions of the struck quarks, and \vec{y}_\perp is the relative distance in the transverse plane between the struck quarks.

Integrating Eq. (12) over the transverse relative distance \vec{y}_\perp produces a delta function $\delta^2(\vec{k}_{1\perp} - \vec{k}'_{1\perp})$, which removes the integration over $\vec{k}'_{1\perp}$. Subsequently, by integrating over the momentum fraction $x_1(x_2)$, one explicitly recovers the standard overlap representation of the unpolarized PDF for the parton $q_2(q_1)$, within the same Fock-sector truncation scheme (see, e.g., Eq. (6) in Ref [95]). We have numerically verified this integral relationship, confirming excellent agreement. This result provides strong evidence for the internal consistency and probabilistic interpretation of the DPDs computed within our BLFQ-based approach.

Similarly, the overlap representation for the DPDs of two longitudinally polarized quarks corresponding to the operator with $\Gamma_{\Delta_q} = \frac{1}{2} \gamma^+ \gamma_5$ can be written as:

$$F_{\Delta q_1 \Delta q_2}(x_1, x_2, \vec{y}_\perp) = \sum_{s_i} (4s_1 \cdot s_2) \int d^2 \vec{k}_{1\perp} d^2 \vec{k}_{2\perp} d^2 \vec{k}'_{1\perp} \\ \times \Psi_{\{x_i, \vec{k}'_{i\perp}, s_i\}}^{\dagger*} \Psi_{\{x_i, \vec{k}_{i\perp}, s_i\}}^\dagger e^{i(\vec{k}'_{1\perp} - \vec{k}_{1\perp}) \cdot \vec{y}_\perp}, \quad (13)$$

where s_1 and s_2 are the light-front helicities of the two struck quarks. A similar procedure applied directly to Eq. 13, which describes the distribution of two longitudinally polarized partons, does not yield the overlap representation of the standard longitudinally polarized PDF g_1 . The correct sum rule relevant in this context

relates instead the polarized PDF of one parton to the polarized-unpolarized DPD, that is, the distribution of a longitudinally polarized parton combined with an unpolarized parton. Therefore, a direct integration check as described after Eq. 12 does not apply here.

IV. NUMERICAL RESULTS

The LFWFs of the proton have been obtained in the BLFQ framework with the basis truncation $N_{\max} = 10$ and $K = 16.5$, along with model parameters $\{m_{u/\text{KE}}, m_{d/\text{KE}}, m_{q/\text{OGE}}, \kappa, \alpha_s, b\} = \{0.300 \text{ GeV}, 0.301 \text{ GeV}, 0.200 \text{ GeV}, 0.34 \text{ GeV}, 1.1 \pm 0.1, 0.6 \text{ GeV}\}$, where $m_{q/\text{K.E.}}$ and $m_{q/\text{OGE}}$ correspond to the quark masses in kinetic energy and OGE interaction terms, and b is the HO scale parameter.

The parameters in our model are determined to reproduce the known nucleon mass and electromagnetic form factors [95, 96]. The LFWFs of the valence Fock sector with these parameters, with an implicit model scale of $\mu_0^2 = 0.195 \pm 0.020 \text{ GeV}^2$ [95, 96], are utilized to derive physical observables and distribution functions of the valence quarks within the proton. Our focus in this work is on investigating the DPDs of the proton using these LFWFs. We insert the valence LFWFs given by Eq. (8) into Eqs. (12) and (13) to compute the valence quark DPDs inside the proton.

A. Unpolarized quark DPDs $F_{q_1 q_2}(x_1, x_2, \vec{y}_\perp)$

The unpolarized quark DPDs, denoted as $F_{q_1 q_2}(x_1, x_2, \vec{y}_\perp)$, quantify the likelihood of identifying two quarks within a hadron, carrying momentum fractions x_1 and x_2 , and separated by a transverse distance \vec{y}_\perp . This probabilistic description is restricted to the physically meaningful kinematic region, more specifically where the sum of the momentum fractions does not exceed unity, $x_1 + x_2 < 1$. This constraint ensures that the calculations obtain support from the chosen basis configurations of BLFQ.

TABLE I. The peak positions and values of unpolarized DPDs F_{du_1} and $F_{u_1 u_2}$ in Fig. 1 and 2.

$ \vec{y}_\perp /\text{fm}$	(x_d, x_{u_1})	values	(x_{u_1}, x_{u_2})	values
0	(0.347, 0.376)	0.102	(0.377, 0.377)	0.122
0.5	(0.333, 0.365)	0.076	(0.366, 0.366)	0.081
1.0	(0.296, 0.343)	0.030	(0.341, 0.341)	0.029
1.5	(0.287, 0.327)	0.009	(0.321, 0.321)	0.009

Figure 1 shows the contour plots depicting the unpolarized DPDs for a down quark (d) and an up quark (u_1)²

² Here, the subscript 1 and 2 for u are just labels since in our

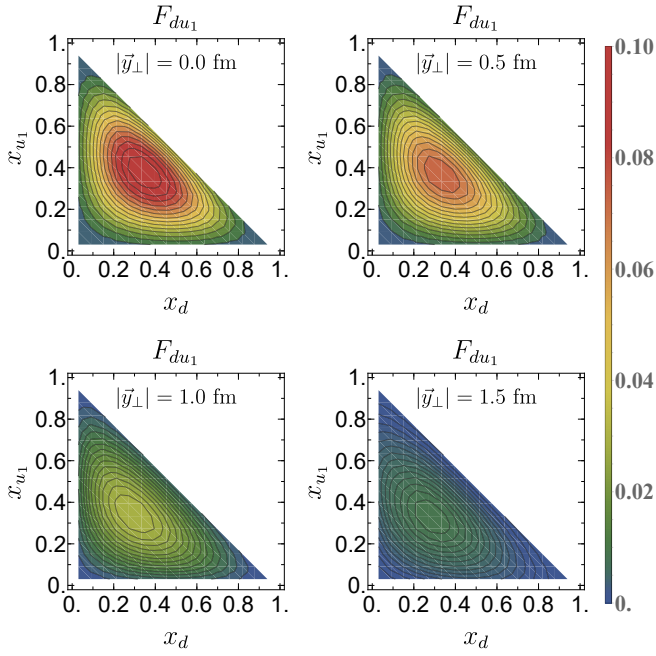


FIG. 1. The unpolarized DPDs $F_{du_1}(x_d, x_{u_1}, \vec{y}_\perp)$ as functions of x_d and x_{u_1} for different values of $|\vec{y}_\perp| = \{0, 0.5, 1.0, 1.5\}$ fm.

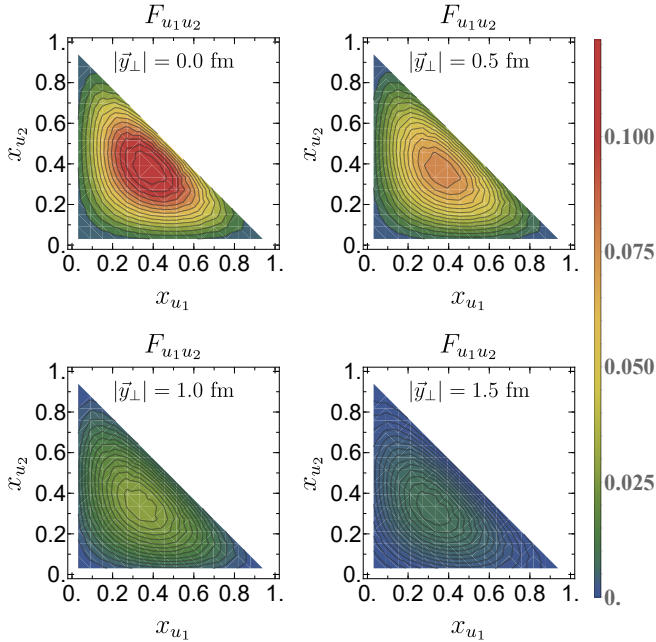


FIG. 2. The unpolarized DPDs $F_{u_1 u_2}(x_{u_1}, x_{u_2}, \vec{y}_\perp)$ as functions of x_{u_1} and x_{u_2} for different values of $|\vec{y}_\perp| = \{0, 0.5, 1.0, 1.5\}$ fm.

calculation those two up quarks are indistinguishable. The only reason to include those subscripts is to stress that here we show only half of the DPDs between d and u quark. Similarly for $F_{u_1 u_2}$ later.

within the proton, plotted against their longitudinal momentum fractions x_d and x_{u_1} . We show the distributions for various transverse distances $|\vec{y}_\perp|$, ranging from $|\vec{y}_\perp| = 0$ fm to $|\vec{y}_\perp| = 1.5$ fm. For ease of visualization, the values corresponding to different colors change from one plot to the other as indicated by the color bars to the right of each plot. Fig. 1 shows that the unpolarized DPDs first increase and then decrease when $x_d + x_{u_1}$ increases, with the peak around $x_d \approx x_{u_1} \approx 0.3$. Table. I explicitly shows the numerical locations of peaks in the unpolarized DPDs. As evident, the peak positions systematically shift toward lower values of x as the transverse distance $|\vec{y}_\perp|$ between the quarks increases. This behavior arises from the weakening of partonic correlations at large transverse separation, where the system approaches a decorrelated regime and low- x configurations become more prominent. Additionally, the table reveals a structural difference between the two flavor combinations. In the $F_{u_1 u_2}$ case, the peak consistently lies along the $x_{u_1} = x_{u_2}$ diagonal, reflecting the symmetry between the two identical u quarks. In contrast, for the F_{du_1} case, the peak position is systematically off-diagonal, with $x_d < x_{u_1}$ at all $|\vec{y}_\perp|$. This asymmetry originates from the small but nonzero mass difference between the u and d quarks in our model, which breaks exact flavor symmetry. As a result, the d quark consistently carries slightly less longitudinal momentum than the u quark, leading to a peak location that lies below the $x_d = x_{u_1}$ diagonal. This asymmetry persists across all transverse separations shown in Fig. 1 and is quantitatively supported by the values in Table I.

Figure 2, which focuses on the interaction between two up quarks u_1 and u_2 , exhibits trends similar to that observed in Fig. 1. However, a subtle shift in the peak positions between the two figures is observed which is more explicit in the large $|\vec{y}_\perp|$ case. The slightly asymmetric patterns for distinguishable (u, d) quarks seen in Fig. 1 that result from our small (u, d) quark mass splitting are replaced by the symmetric patterns seen in Fig. 2 (and corresponding results in Table. I) that reflect the inherent indistinguishability of the (u_1, u_2) quarks. This variation is attributed to the slight numerical differences in the masses (1 MeV) between the up and down quarks in our calculations, which breaks the isospin symmetry. We also observe that for a fixed $|\vec{y}_\perp|$, the distribution $F_{u_1 u_2}$ has a larger magnitude than that of the F_{du_1} , which signifies a stronger correlation between the two u quarks than that between the d and u quarks in the proton.

In Fig. 3, we show the contour plot of the unpolarized DPDs F_{du_1} as functions of x_{u_1} and \vec{y}_\perp with fixed values of $x_d = \{0.5, 4.5, 7.5, 11.5\}/16.5$. The DPDs achieve their maximum values when the relative distance between the two quarks is zero. As x_d increases the peak value of the distribution first rises and then falls off. We observe that the distribution exhibits an approximate symmetry over x_{u_1} when x_d is at its smallest value. However, this symmetry is broken as x_d increases. Similar observations can also be noticed in Fig. 4, where the unpolarized DPDs

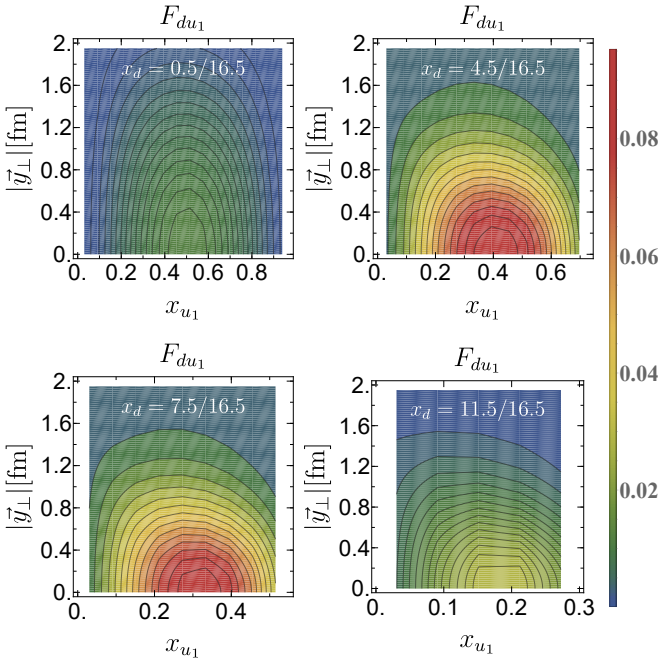


FIG. 3. The unpolarized DPDs $F_{du_1}(x_d, x_{u_1}, \vec{y}_\perp)$ as functions of x_{u_1} and $|\vec{y}_\perp|$ for different values of $x_d = \{0.5, 4.5, 7.5, 11.5\}/16.5$.

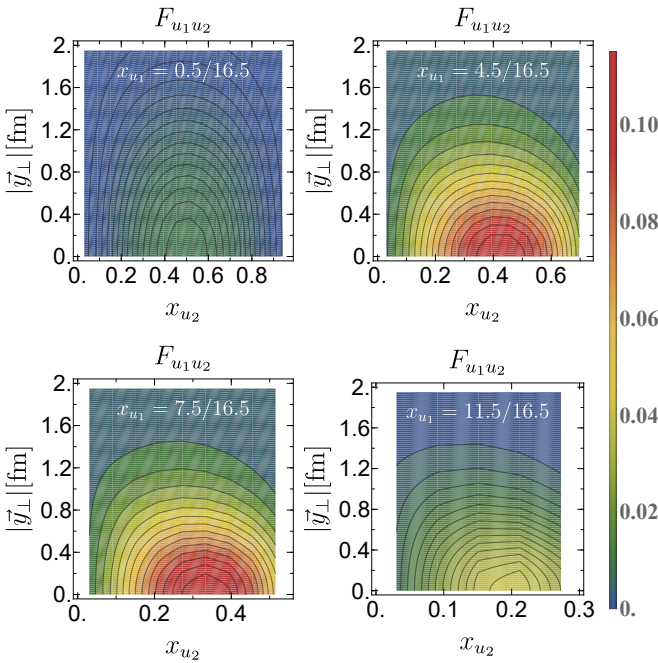


FIG. 4. The unpolarized DPDs $F_{u_1 u_2}(x_{u_1} x_{u_2}, \vec{y}_\perp)$ as functions of x_{u_2} and $|\vec{y}_\perp|$ for different values of $x_{u_1} = \{0.5, 4.5, 7.5, 11.5\}/16.5$.

$F_{u_1 u_2}$ are shown as functions of x_{u_2} and \vec{y}_\perp with fixed values of x_{u_1} .

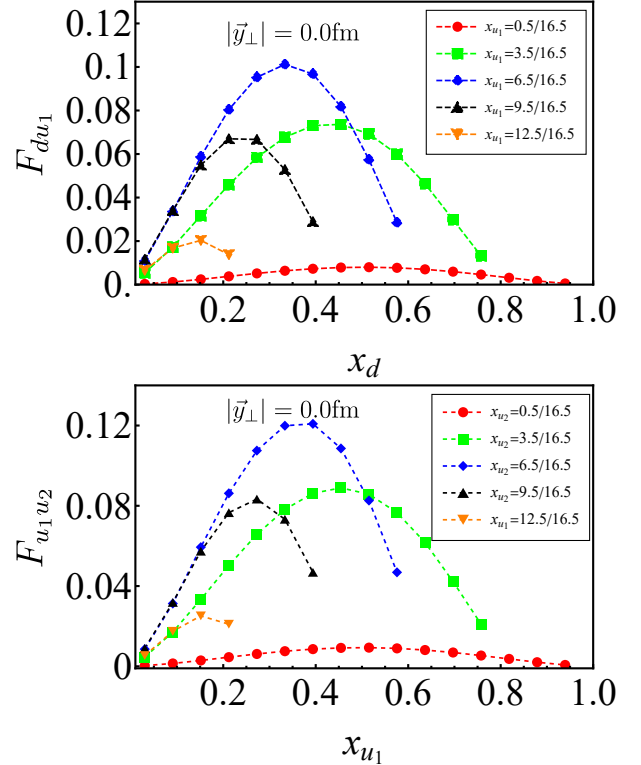


FIG. 5. The unpolarized DPDs, $F_{du_1}(x_d, x_{u_1}, \vec{y}_\perp)$ (upper panel) and $F_{u_1 u_2}(x_{u_1}, x_{u_2}, \vec{y}_\perp)$ (lower panel), as functions of $x_d(x_{u_1})$ for different values of $x_{u_1}(x_{u_2}) = \{0.5, 3.5, 6.5, 9.5, 12.5\}/16.5$ and fixed $|\vec{y}_\perp| = 0$ fm.

In Fig. 5, we show the 2D plots of the unpolarized DPDs $F_{du_1}(F_{u_1 u_2})$ as functions of x_d (x_{u_1}) for fixed values of x_{u_1} (x_{u_2}) at the transverse distance of $|\vec{y}_\perp| = 0$ fm. We observe that as the value of x_{u_1} (x_{u_2}) increases the peak of the curve shifts towards lower values of x_d (x_{u_1}) and simultaneously the magnitude of the peak increases first and then decreases.

In Fig. 6, we plot the unpolarized DPDs $F_{du_1}(F_{u_1 u_2})$ against the transverse distance $|\vec{y}_\perp|$ with fixed x_{u_1} (x_{u_2}) and different x_d (x_{u_1}), and we observe that as the distance between the two struck quarks increases, the probability of finding them decreases. With x_{u_1} (x_{u_2}) = 0.5/16.5, the magnitude of the distribution reaches its maximum around x_d (x_{u_1}) ≈ 0.5. Note that if we further increase the fixed value of x_{u_1} (x_{u_2}), the maximum of the distribution appears at x_d (x_{u_1}) < 0.5, as can be seen in Figs. 3 and 4.

B. Polarized quark DPDs $F_{\Delta q_1 \Delta q_2}(x_1, x_2, \vec{y}_\perp)$

The polarized DPDs $F_{\Delta q_1 \Delta q_2}(x_1, x_2, \vec{y}_\perp)$ describe the difference between the probabilities of finding the two quarks with helicities both aligned and both anti-aligned

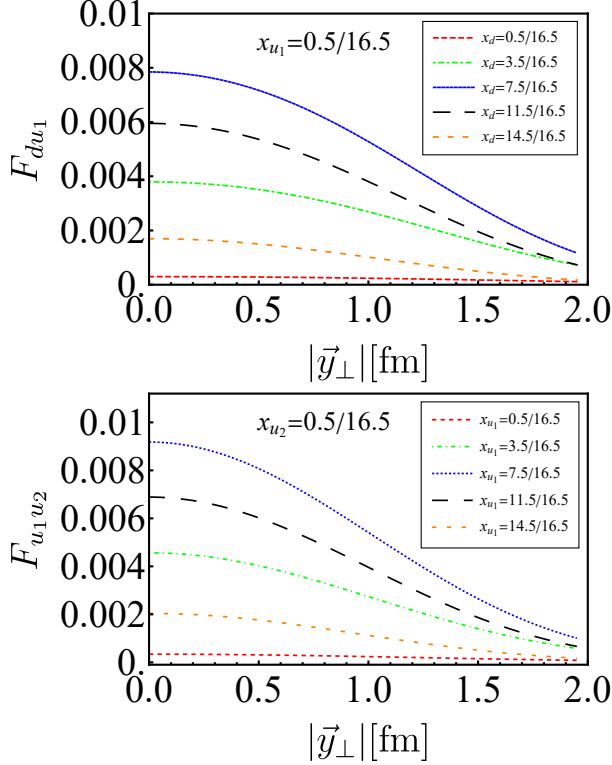


FIG. 6. The unpolarized DPDs, $F_{du_1}(x_d, x_{u_1}, \vec{y}_\perp)$ (upper panel) and $F_{u_1 u_2}(x_{u_1}, x_{u_2}, \vec{y}_\perp)$ (lower panel), as functions of $|\vec{y}_\perp|$ for different values of $x_d(x_{u_1}) = \{0.5, 3.5, 7.5, 11.5, 14.5\}/16.5$ and fixed value of $x_{u_1}(x_{u_2}) = 0.5/16.5$.

to the proton helicity. Thus it gives a measure for the longitudinal quark polarization.

TABLE II. The peak positions and values of polarized DPDs $F_{\Delta d \Delta u_1}$ and $F_{\Delta u_1 \Delta u_2}$ in Fig. 7 and 8.

$ \vec{y}_\perp /\text{fm}$	(x_d, x_{u_1})	values	(x_{u_1}, x_{u_2})	values
0	(0.346, 0.356)	-0.066	(0.377, 0.377)	0.022
0.5	(0.335, 0.354)	-0.032	(0.374, 0.374)	0.015
1.0	(0.344, 0.349)	-0.007	(0.356, 0.356)	0.006
1.5	(0.330, 0.328)	-0.002	(0.322, 0.322)	0.002

Figure 7 illustrates the polarized DPDs of d and u_1 inside the proton as functions of their respective longitudinal momentum fractions x_d and x_{u_1} at transverse distance ranging from $|\vec{y}_\perp| = 0 \text{ fm}$ to $|\vec{y}_\perp| = 1.5 \text{ fm}$. Unlike the unpolarized distribution, F_{du_1} , we find that when the struck quarks are longitudinally polarized, the double parton distributions relating up and down quarks are negative. We again find that the magnitudes of the polarized DPDs first increase and then decrease when $x_d + x_{u_1}$ increases, with the peak around $x_d \approx x_{u_1} \approx 0.3$. A similar observation is also noticed for the polarized DPD of u_1 and u_2 quarks in Fig. 8. However, in contrast with $F_{\Delta d \Delta u_1}$, $F_{\Delta u_1 \Delta u_2}$ are positive, similar to the unpolarized

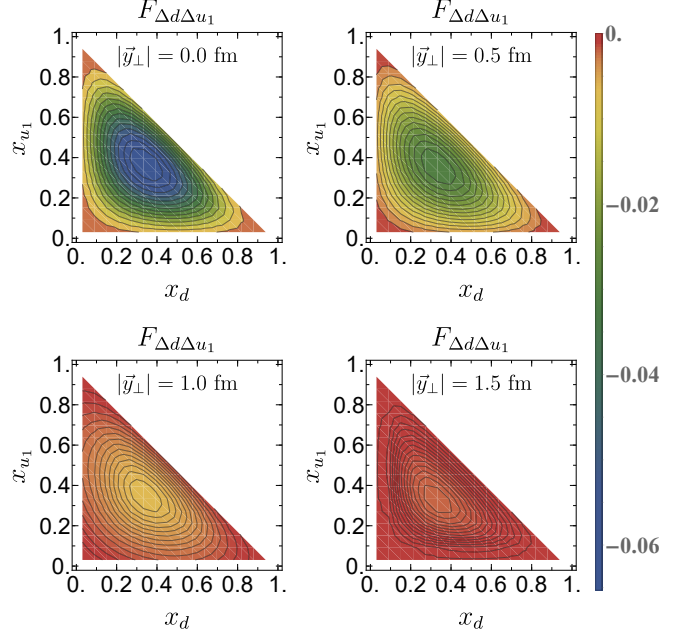


FIG. 7. The polarized DPDs $F_{\Delta d \Delta u_1}(x_d, x_{u_1}, \vec{y}_\perp)$ as functions of x_d and x_{u_1} for different values of $|\vec{y}_\perp| = \{0, 0.5, 1.0, 1.5\} \text{ fm}$.

distributions shown in Fig. 2. Here we observe a clear effect of the longitudinal polarization from the different signs of $F_{\Delta d \Delta u_1}$ and $F_{\Delta u_1 \Delta u_2}$ compared with the same sign for the unpolarized case. Similar to the unpolarized DPDs, Table. II presents numerical peak positions for the polarized DPDs, again indicating a clear trend of peak locations moving toward smaller x -values with increasing $|\vec{y}_\perp|$.

In Fig. 9, we show the contour plot of the polarized DPDs $F_{\Delta d \Delta u_1}$ as functions of x_{u_1} and $|\vec{y}_\perp|$ with fixed values of $x_d = \{0.5, 4.5, 7.5, 11.5\}/16.5$. Similar to the unpolarized DPDs, we observe the maxima of the magnitude of the DPDs when the relative distance between the two quarks vanishes. Figure 10 shows the polarized DPDs $F_{\Delta u_1 \Delta u_2}$ as functions of x_{u_2} and $|\vec{y}_\perp|$ with fixed values of x_{u_1} .

In Fig. 11, we plot the polarized DPDs as functions of x_d (x_{u_1}) for fixed values of x_{u_1} (x_{u_2}) at the transverse distance of $|\vec{y}_\perp| = 0 \text{ fm}$. The qualitative behavior is similar to the unpolarized case as shown in Fig. 5. As the value of x_{u_1} (x_{u_2}) increases, the peak position of the curve shifts towards lower values of x_d (x_{u_1}) and simultaneously the magnitude of the peak increases first and then decreases.

In Fig. 12, we show the polarized DPDs as functions of $|\vec{y}_\perp|$, while keeping x_{u_1} (x_{u_2}) fixed and varying the values of x_d (x_{u_1}) for different curves. Our analysis reveals that $|F_{\Delta d \Delta u_1}|$ exceeds $|F_{\Delta u_1 \Delta u_2}|$, indicating a stronger correlation between longitudinally polarized down and up quarks compared to that between longitudinally polarized up and up quarks within the proton.

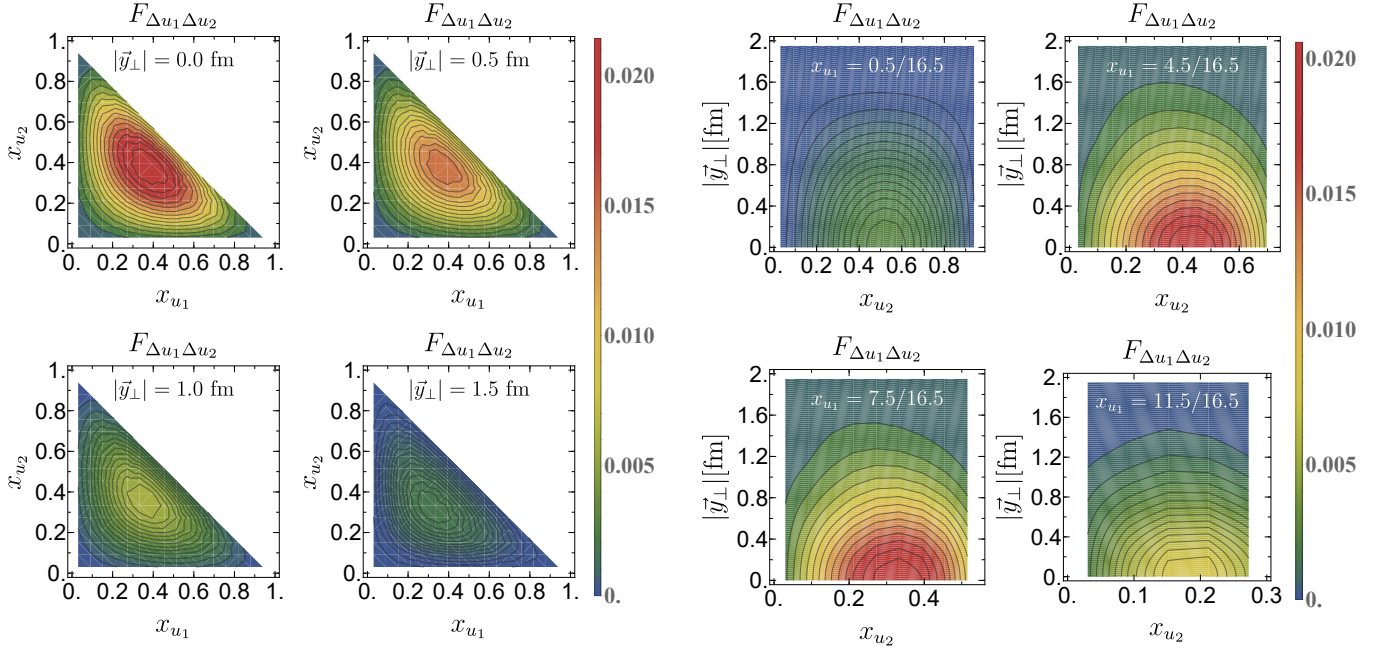


FIG. 8. The polarized DPDs $F_{\Delta u_1 \Delta u_2}(x_{u_1}, x_{u_2}, \vec{y}_\perp)$ as functions of x_{u_1} and x_{u_2} for different values of $|\vec{y}_\perp| = \{0, 0.5, 1.0, 1.5\}$ fm.

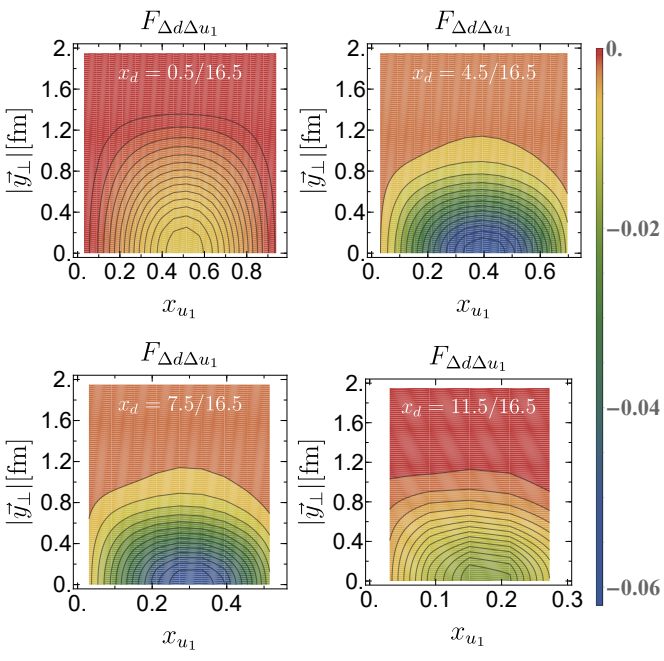


FIG. 9. The polarized DPDs $F_{\Delta d \Delta u_1}(x_d, x_{u_1}, \vec{y}_\perp)$ as functions of x_{u_1} and $|\vec{y}_\perp|$ for different values of $x_d = \{0.5, 4.5, 7.5, 11.5\}/16.5$.

FIG. 10. The polarized DPDs $F_{\Delta u_1 \Delta u_2}(x_{u_1}, x_{u_2}, \vec{y}_\perp)$ as functions of x_{u_2} and $|\vec{y}_\perp|$ for different value of $x_{u_1} = \{0.5, 4.5, 7.5, 11.5\}/16.5$.

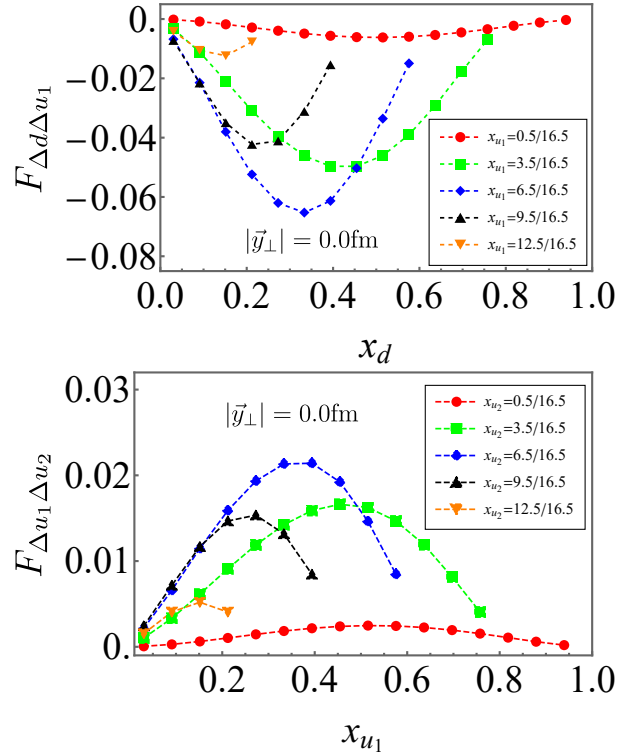


FIG. 11. The polarized DPDs, $F_{\Delta d \Delta u_1}(x_d, x_{u_1}, \vec{y}_\perp)$ (upper panel) and $F_{\Delta u_1 \Delta u_2}(x_{u_1}, x_{u_2}, \vec{y}_\perp)$ (lower panel), as functions of $x_d(x_{u_1})$ for different values of $x_{u_1}(x_{u_2}) = \{0.5, 3.5, 6.5, 9.5, 12.5\}/16.5$ and fixed $|\vec{y}_\perp| = 0$ fm.

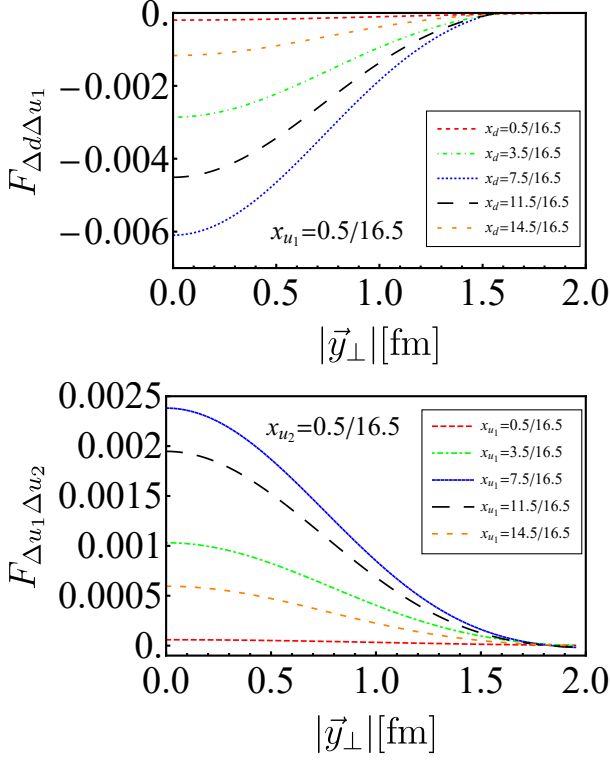


FIG. 12. The polarized DPDs, $F_{\Delta d \Delta u_1}(x_d, x_{u_1}, \vec{y}_\perp)$ (upper panel) and $F_{\Delta u_1 \Delta u_2}(x_d, x_{u_1}, \vec{y}_\perp)$ (lower panel), as functions of $|\vec{y}_\perp|$ for different values of $x_d(x_{u_1}) = \{0.5, 3.5, 7.5, 11.5, 14.5\}/16.5$ and fixed values of $x_{u_1}(x_{u_2}) = 0.5/16.5$.

C. DPDs in momentum space

The Fourier transform allows the conversion of DPDs from coordinate space to momentum space, as represented by the following equation:

$$\int \frac{d^2 \vec{y}_\perp}{(2\pi)^2} e^{-i \vec{k}_\perp \cdot \vec{y}_\perp} F(x_1, x_2, \vec{y}_\perp) = \tilde{F}(x_1, x_2, \vec{k}_\perp), \quad (14)$$

where $\tilde{F}(x_1, x_2, \vec{k}_\perp)$ denotes the DPDs in momentum space. The variable \vec{k}_\perp represents the difference in transverse momenta between the struck quarks in the initial and final states, expressed as $\vec{k}_\perp = \vec{k}_{1\perp} - \vec{k}_{2\perp} = \vec{k}_{2\perp} - \vec{k}_{1\perp}$.

In Fig. 13, we present the unpolarized DPDs in momentum space, fixing $x_{u_1}(x_{u_2})$ and plotting them as functions of $x_d(x_{u_1})$ for various values of $|\vec{k}_\perp|$. As $|\vec{k}_\perp|$ increases, we notice that the peak of the distribution not only gets smaller but also moves slightly towards lower values of x . At $|\vec{k}_\perp| = 0$, the peak values of \tilde{F}_{du_1} and $\tilde{F}_{u_1 u_2}$ are almost identical. However, for non-zero $|\vec{k}_\perp|$, the peak of \tilde{F}_{du_1} is slightly higher than that of $\tilde{F}_{u_1 u_2}$. The decrease of the peak value is significant, dropping from its initial value (0.10553) to a much lower (0.00074)

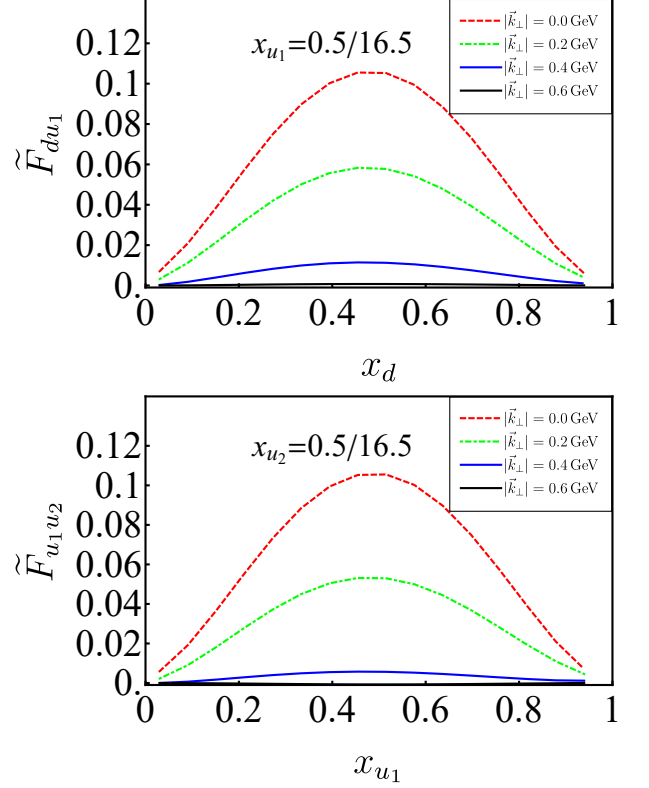


FIG. 13. The unpolarized DPDs, $\tilde{F}_{du_1}(x_d, x_{u_1}, |\vec{k}_\perp|)$ (upper panel) and $\tilde{F}_{u_1 u_2}(x_d, x_{u_1}, |\vec{k}_\perp|)$ (lower panel) as functions of $x_d(x_{u_1})$ for different values of $|\vec{k}_\perp| = \{0, 0.2, 0.4, 0.6\}$ GeV and fixed $x_{u_1}(x_{u_2}) = 0.5/16.5$.

one as $|\vec{k}_\perp|$ increases from 0 to 0.6 GeV for \tilde{F}_{du_1} . The general trends of our findings are consistent with predictions from the bag model [48] and the constituent quark model [49, 51]. Similarly, the polarized DPDs depicted in Fig. 14 exhibit trends akin to those in Fig. 13, with $\tilde{F}_{\Delta d \Delta u_1}$ having negative values, in contrast to $\tilde{F}_{\Delta u_1 \Delta u_2}$.

We further analyze the $|\vec{k}_\perp|$ dependence by evaluating the ratio \tilde{R} defined as,

$$\begin{aligned} \tilde{R}_{q_1 q_2}(x_1, k_\perp) &= \frac{\tilde{F}_{q_1 q_2}(x_1, x_2 = 0.4, k_\perp)}{\tilde{F}_{q_1 q_2}(x_1 = 0.4, x_2 = 0.4, k_\perp)}, \\ \tilde{R}_{\Delta q_1 \Delta q_2}(x_1, k_\perp) &= \frac{\tilde{F}_{\Delta q_1 \Delta q_2}(x_1, x_2 = 0.4, k_\perp)}{\tilde{F}_{\Delta q_1 \Delta q_2}(x_1 = 0.4, x_2 = 0.4, k_\perp)}. \end{aligned} \quad (15)$$

This ratio was studied in the bag model [48] and the constituent quark model [49, 51] to test the violation of the factorization of the DPDs into functions of the transverse separation and functions of the longitudinal momentum fractions. This ratio should be independent of $|\vec{k}_\perp|$ if the factorization holds exactly and thus, the magnitude of $|\vec{k}_\perp|$ dependence of this ratio would be a measure of the violation of the factorization in x and \vec{k}_\perp .

In Figs. 15 and 16, we present the unpolarized and

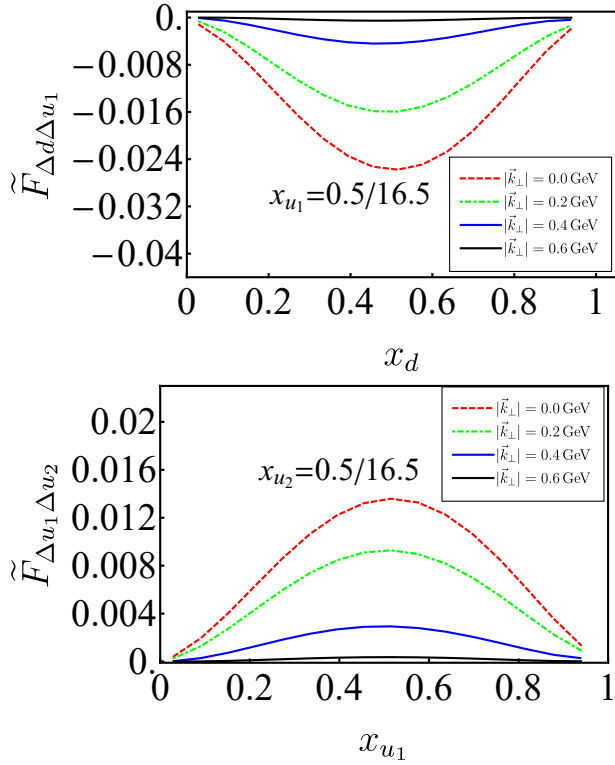


FIG. 14. The polarized DPDs, $\tilde{F}_{\Delta d \Delta u_1}(x_d, x_{u_1}, |\vec{k}_\perp|)$ (upper panel) and $\tilde{F}_{\Delta u_1 \Delta u_2}(x_{u_1}, x_{u_2}, |\vec{k}_\perp|)$ (lower panel) as functions of x_d (x_{u_1}) for different values of $|\vec{k}_\perp| = \{0, 0.2, 0.4, 0.6\}$ GeV and fixed $x_{u_1}(x_{u_2}) = 0.5/16.5$.

polarized ratios of the DPDs, respectively, plotted as functions of the longitudinal momentum fraction at different values of $|\vec{k}_\perp|$. To facilitate comparison with the ratios $\tilde{R}_{u_1 u_2}$ and $\tilde{R}_{\Delta u_1 \Delta u_2}$ calculated in the constituent quark model [51], we use 0.4 as the constant parameter in the definition of these ratios, as with Eqs. (3.9, 3.10) in Ref [51]. The most notable observation from these plots of the results from our approach is the significant increase in the factorization violation as $|\vec{k}_\perp|$ increases, particularly evident in the high x_{u_1} region, which is more pronounced in the polarized distributions, shown in Fig. 16. Both in the constituent quark model [51] and in our results the violation of factorization increases as $|\vec{k}_\perp|$ increases, though the violation is more pronounced with our results. When compared with the ratios obtained in the constituent quark model from Ref. [51], our results show a shift towards larger x_{u_1} values for both the unpolarized and polarized distributions. Furthermore, in the lower x_{u_1} range, the unpolarized ratios exhibit significantly greater factorization violations compared to the polarized ones. This is evident from the larger separations among the lines for $\tilde{R}_{u_1 u_2}$ in Fig. 15, in contrast to the smaller separations among the lines for $\tilde{R}_{\Delta u_1 \Delta u_2}$ in Fig. 16. In fact, the polarized ratio, especially $\tilde{R}_{\Delta u_1 \Delta u_2}$, remains nearly constant across different values of \vec{k}_\perp in

the low x_{u_1} region.

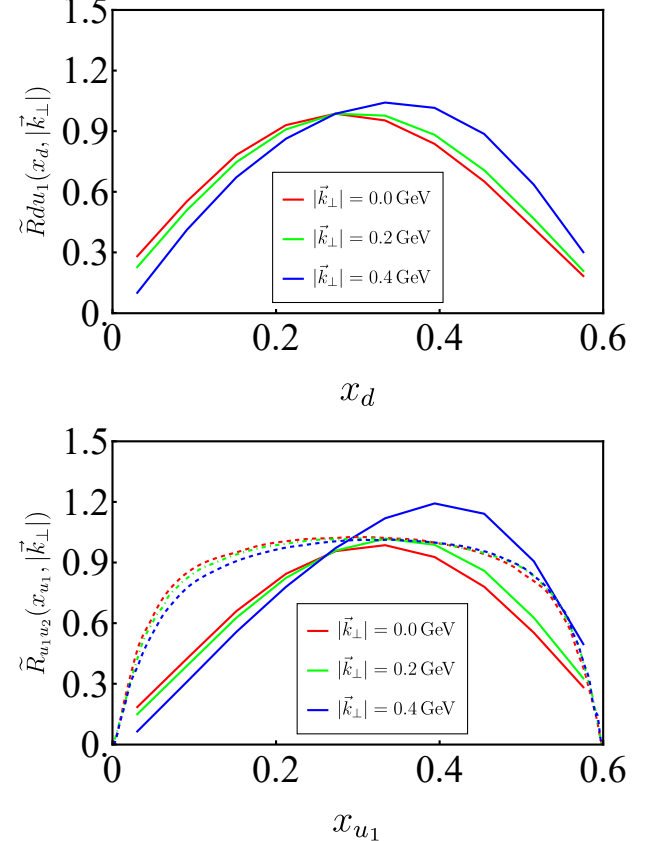


FIG. 15. The unpolarized DPDs ratio \tilde{R}_{du_1} (upper panel) and $\tilde{R}_{u_1 u_2}$ (lower panel) as defined in Eq. (15) are plotted as functions of $x_d(x_{u_1})$, for three values of $|\vec{k}_\perp| = \{0, 0.2, 0.4\}$ GeV. Our results (solid lines) for $\tilde{R}_{u_1 u_2}$ are compared with those from the constituent quark model (dashed lines) [51].

V. SUMMARY AND OUTLOOKS

Basis light-front quantization (BLFQ) is a fully relativistic and nonperturbative method for solving quantum field theory based on the light-front Hamiltonian. Using a recently proposed effective light-front Hamiltonian for the baryon within BLFQ, we presented a study of double parton distributions (DPDs) of the proton. With quarks being the only degrees of freedom, the effective Hamiltonian incorporates confinement in both the transverse and longitudinal directions and a one-gluon exchange interaction for the constituent valence quarks suitable for low-resolution properties. We obtained the light-front wave functions (LFWFs) as the eigenvectors of this effective Hamiltonian in the leading Fock sector. Employing the resulting LFWFs, we calculated the unpolarized and longitudinally polarized quark-quark double parton distributions of the proton.

Our approach enables a direct investigation into the

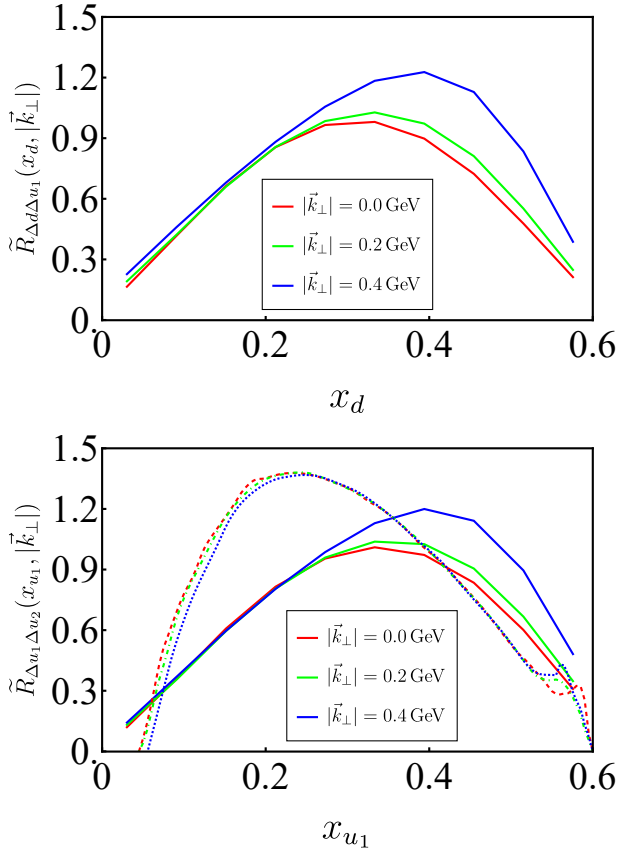


FIG. 16. The polarized DPDs ratio $\tilde{R}_{\Delta d \Delta u_1}$ (upper panel) and $\tilde{R}_{\Delta u_1 \Delta u_2}$ (lower panel) as defined in Eq. (15) are plotted as functions of $x_d(x_{u_1})$, for three values of $|\vec{k}_\perp| = \{0, 0.2, 0.4\}$ GeV. Our results (solid lines) for $\tilde{R}_{\Delta u_1 \Delta u_2}$ are compared with those from the constituent quark model (dashed lines) [51].

correlation between quark momentum fractions x_1 and x_2 , and their transverse separation \vec{y}_\perp , without assuming any factorization between them. Our results reveal strong correlations among these variables and are promising for enhancing model parametrizations of baryon DPDs.

All unpolarized DPDs are positive, while those involving a down struck quark are negative for polarized DPDs. We observed that the correlation is stronger between two unpolarized up quarks compared to an up and a down quark ($F_{du_1} < F_{u_1 u_2}$). Conversely, in the polarized case, the correlation is stronger between polarized down and up quarks than between two polarized up quarks within the proton ($|F_{\Delta d \Delta u_1}| > |F_{\Delta u_1 \Delta u_2}|$). Furthermore, we presented the DPDs in momentum space, finding consistency with the constituent quark model broadly. Our calculations do not support the $x - \vec{k}_\perp$ factorization of the DPDs, which is often employed in various phenomenological applications and experimental programs, including those at the Large Hadron Collider.

This study aims to explore the double parton structure of the proton within its valence Fock sector. Fu-

ture investigations will include higher Fock states, aiming to uncover correlations among valence quarks, sea quarks, and gluons within the proton. The accumulation of high-precision data on double parton scattering from hadron-hadron collision experiments will provide valuable insights into a detailed picture of the multi-parton structure of the proton. By employing QCD evolution equations for DPDs, we also intend to evolve these distributions to higher energy scales for comparison with double parton scattering cross-sections observed in hadron-hadron collision experiments. Upcoming research will also examine double parton correlations in heavy baryon systems, exploring potential distinctions from the proton.

ACKNOWLEDGMENTS

S. N. is supported by the Senior Scientist Program funded by Gansu Province, Grant No. 23JDKA0005. C. M. thanks the Chinese Academy of Sciences President's International Fellowship Initiative for the support via Grants No. 2021PM0023. C. M. is also supported by new faculty start up funding by the Institute of Modern Physics, Chinese Academy of Sciences, Grant No. E129952YR0. X.L. is supported by the National Natural Science Foundation of China under Grants No. 12335001 and No. 12247101, National Key Research and Development Program of China under Contract No. 2020YFA0406400, the 111 Project under Grant No. B20063, the fundamental Research Funds for the Central Universities, and the project for top-notch innovative talents of Gansu province. X. Z. is supported by new faculty startup funding by the Institute of Modern Physics, Chinese Academy of Sciences, by Key Research Program of Frontier Sciences, Chinese Academy of Sciences, Grant No. ZDBS-LY-7020, by the Foundation for Key Talents of Gansu Province, by the Central Funds Guiding the Local Science and Technology Development of Gansu Province, Grant No. 22ZY1QA006, by international partnership program of the Chinese Academy of Sciences, Grant No. 016GJHZ2022103FN, by National Key R&D Program of China, Grant No. 2023YFA1606903, by the Strategic Priority Research Program of the Chinese Academy of Sciences, Grant No. XDB34000000, Grant No. 25RCKA008, by the Senior Scientist Program funded by Gansu Province, and by the National Natural Science Foundation of China under Grant No. 12375143. J. P. V. is supported by the Department of Energy under Grant No. DE-SC0023692. This research is supported by Gansu International Collaboration and Talents Recruitment Base of Particle Physics (2023–2027). A major portion of the computational resources were also provided by Sugon Advanced Computing Center. T. P. is supported by Education Department of Gansu Province for Excellent Graduate Student “Innovation Star” under Grant No. 2025CXZX-043. This research is supported by Gansu International Collaboration and Talents Recruitment Base of Particle Physics

(2023–2027). A major portion of the computational re-

sources were also provided by Sugon Advanced Computing Center.

-
- [1] D. E. Soper, Parton distribution functions, Nucl. Phys. B Proc. Suppl. 53 (1997) 69–80. [arXiv:hep-lat/9609018](https://arxiv.org/abs/hep-lat/9609018), doi:10.1016/S0920-5632(96)00600-7.
- [2] P. Bartalini, J. R. Gaunt (Eds.), Multiple Parton Interactions at the LHC, Vol. 29, WSP, 2019. doi:10.1142/10646.
- [3] A. Tumasyan, et al., Observation of same-sign WW production from double parton scattering in proton-proton collisions at $\sqrt{s} = 13$ TeV, Phys. Rev. Lett. 131 (2023) 091803. [arXiv:2206.02681](https://arxiv.org/abs/2206.02681), doi:10.1103/PhysRevLett.131.091803.
- [4] S. Leontsinis, Observation of triple J/ψ meson production in proton-proton collisions at $\sqrt{s}=13$ TeV, Rev. Mex. Fis. Suppl. 3 (3) (2022) 0308046. doi:10.31349/SuplRevMexFis.3.0308046.
- [5] A. Tumasyan, et al., Measurement of double-parton scattering in inclusive production of four jets with low transverse momentum in proton-proton collisions at $\sqrt{s} = 13$ TeV, JHEP 01 (2022) 177. [arXiv:2109.13822](https://arxiv.org/abs/2109.13822), doi:10.1007/JHEP01(2022)177.
- [6] R. Aaij, et al., Observation of Enhanced Double Parton Scattering in Proton-Lead Collisions at $\sqrt{s_{NN}} = 8.16$ TeV, Phys. Rev. Lett. 125 (21) (2020) 212001. [arXiv:2007.06945](https://arxiv.org/abs/2007.06945), doi:10.1103/PhysRevLett.125.212001.
- [7] A. M. Sirunyan, et al., Evidence for WW production from double-parton interactions in proton–proton collisions at $\sqrt{s} = 13$ TeV, Eur. Phys. J. C 80 (1) (2020) 41. [arXiv:1909.06265](https://arxiv.org/abs/1909.06265), doi:10.1140/epjc/s10052-019-7541-6.
- [8] I. Belyaev, D. Savrina, Study of double parton scattering processes with heavy quarks, Adv. Ser. Direct. High Energy Phys. 29 (2018) 141–157. [arXiv:1711.10877](https://arxiv.org/abs/1711.10877), doi:10.1142/9789813227767_0008.
- [9] A. M. Sirunyan, et al., Constraints on the double-parton scattering cross section from same-sign W boson pair production in proton-proton collisions at $\sqrt{s} = 8$ TeV, JHEP 02 (2018) 032. [arXiv:1712.02280](https://arxiv.org/abs/1712.02280), doi:10.1007/JHEP02(2018)032.
- [10] L. An, Measurements of soft QCD and double parton scattering at LHCb, in: 5th Large Hadron Collider Physics Conference, 2017. [arXiv:1708.09773](https://arxiv.org/abs/1708.09773).
- [11] S. Koshkarev, S. Groote, Double J/ψ production as a test of parton momentum correlations in double parton scattering, Phys. Lett. B 847 (2023) 138296. [arXiv:2208.13429](https://arxiv.org/abs/2208.13429), doi:10.1016/j.physletb.2023.138296.
- [12] R. Kirschner, Generalized Lipatov-Altarelli-Parisi Equations and Jet Calculus Rules, Phys. Lett. B 84 (1979) 266–270. doi:10.1016/0370-2693(79)90300-9.
- [13] V. Shelest, A. Snigirev, G. Zinovjev, Gazing into the multiparton distribution equations in qcd, Physics Letters B 113 (4) (1982) 325–328. doi:[https://doi.org/10.1016/0370-2693\(82\)90049-1](https://doi.org/10.1016/0370-2693(82)90049-1). URL <https://www.sciencedirect.com/science/article/pii/0370269382900491>
- [14] G. m. Zinovev, A. m. Snigirev, V. p. Shelest, EQUATIONS FOR MANY PARTON DISTRIBUTIONS IN QUANTUM CHROMODYNAMICS, Theor. Math. Phys. 51 (1982) 523–528. doi:10.1007/BF01017270.
- [15] A. M. Snigirev, Double parton distributions in the leading logarithm approximation of perturbative QCD, Phys. Rev. D 68 (2003) 114012. [arXiv:hep-ph/0304172](https://arxiv.org/abs/hep-ph/0304172), doi:10.1103/PhysRevD.68.114012.
- [16] V. L. Korotkikh, A. M. Snigirev, Double parton correlations versus factorized distributions, Phys. Lett. B 594 (2004) 171–176. [arXiv:hep-ph/0404155](https://arxiv.org/abs/hep-ph/0404155), doi:10.1016/j.physletb.2004.05.012.
- [17] F. A. Ceccopieri, An update on the evolution of double parton distributions, Phys. Lett. B 697 (2011) 482–487. [arXiv:1011.6586](https://arxiv.org/abs/1011.6586), doi:10.1016/j.physletb.2011.02.047.
- [18] F. A. Ceccopieri, A second update on double parton distributions, Phys. Lett. B 734 (2014) 79–85. [arXiv:1403.2167](https://arxiv.org/abs/1403.2167), doi:10.1016/j.physletb.2014.05.015.
- [19] M. Mekhfi, Correlations in Color and Spin in Multiparton Processes, Phys. Rev. D 32 (1985) 2380. doi:10.1103/PhysRevD.32.2380.
- [20] M. Mekhfi, X. Artru, Sudakov Suppression of Color Correlations in Multiparton Scattering, Phys. Rev. D 37 (1988) 2618–2622. doi:10.1103/PhysRevD.37.2618.
- [21] A. V. Manohar, W. J. Waalewijn, A QCD Analysis of Double Parton Scattering: Color Correlations, Interference Effects and Evolution, Phys. Rev. D 85 (2012) 114009. [arXiv:1202.3794](https://arxiv.org/abs/1202.3794), doi:10.1103/PhysRevD.85.114009.
- [22] M. Diehl, F. Fabry, A. Vladimirov, Two-loop evolution kernels for colour dependent double parton distributions, JHEP 05 (2023) 067. [arXiv:2212.11843](https://arxiv.org/abs/2212.11843), doi:10.1007/JHEP05(2023)067.
- [23] F. Abe, et al., Double parton scattering in $\bar{p}p$ collisions at $\sqrt{s} = 1.8$ TeV, Phys. Rev. D 56 (1997) 3811–3832. doi:10.1103/PhysRevD.56.3811.
- [24] V. M. Abazov, et al., Study of double parton interactions in diphoton + dijet events in $p\bar{p}$ collisions at $\sqrt{s} = 1.96$ TeV, Phys. Rev. D 93 (5) (2016) 052008. [arXiv:1512.05291](https://arxiv.org/abs/1512.05291), doi:10.1103/PhysRevD.93.052008.
- [25] R. Aaij, et al., Measurement of the J/ψ pair production cross-section in pp collisions at $\sqrt{s} = 13$ TeV, JHEP 06 (2017) 047, [Erratum: JHEP 10, 068 (2017)]. [arXiv:1612.07451](https://arxiv.org/abs/1612.07451), doi:10.1007/JHEP06(2017)047.
- [26] M. Aaboud, et al., Measurement of J/ψ production in association with a W^\pm boson with pp data at 8 TeV, JHEP 01 (2020) 095. [arXiv:1909.13626](https://arxiv.org/abs/1909.13626), doi:10.1007/JHEP01(2020)095.
- [27] R. Abdul Khalek, et al., Science Requirements and Detector Concepts for the Electron-Ion Collider: EIC Yellow Report, Nucl. Phys. A 1026 (2022) 122447. [arXiv:2103.05419](https://arxiv.org/abs/2103.05419), doi:10.1016/j.nuclphysa.2022.122447.
- [28] D. P. Anderle, et al., Electron-ion collider in China, Front. Phys. (Beijing) 16 (6) (2021) 64701. [arXiv:2102.09222](https://arxiv.org/abs/2102.09222), doi:10.1007/s11467-021-1062-0.
- [29] J. Katich, et al., Measurement of the Target-Normal Single-Spin Asymmetry in Deep-Inelastic Scattering from the Reaction ${}^3\text{He}^\dagger(e, e')X$, Phys. Rev. Lett. 113 (2) (2014) 022502. [arXiv:1311.0197](https://arxiv.org/abs/1311.0197), doi:10.1103/

- [PhysRevLett.113.022502](#).
- [30] A. Metz, D. Pitonyak, A. Schafer, M. Schlegel, W. Vogelsang, J. Zhou, Single-spin asymmetries in inclusive deep inelastic scattering and multiparton correlations in the nucleon, Phys. Rev. D 86 (2012) 094039. [arXiv:1209.3138](#), [doi:10.1103/PhysRevD.86.094039](#).
- [31] A. Afanasev, M. Strikman, C. Weiss, Transverse target spin asymmetry in inclusive DIS with two-photon exchange, Phys. Rev. D 77 (2008) 014028. [arXiv:0709.0901](#), [doi:10.1103/PhysRevD.77.014028](#).
- [32] N. Paver, D. Treleani, Multi - Quark Scattering and Large p_T Jet Production in Hadronic Collisions, Nuovo Cim. A 70 (1982) 215. [doi:10.1007/BF02814035](#).
- [33] M. Mekhfi, Multiparton processes: An application to the double drell-yan mechanism, Phys. Rev. D 32 (1985) 2371–2379. [doi:10.1103/PhysRevD.32.2371](#). URL <https://link.aps.org/doi/10.1103/PhysRevD.32.2371>
- [34] T. Sjöstrand, M. Van Zijl, Multiple parton-parton interactions in an impact parameter picture, Physics Letters B 188 (1) (1987) 149–154. [doi:https://doi.org/10.1016/0370-2693\(87\)90722-2](#). URL <https://www.sciencedirect.com/science/article/pii/0370269387907222>
- [35] B. Blok, Y. Dokshitzer, L. Frankfurt, M. Strikman, The Four jet production at LHC and Tevatron in QCD, Phys. Rev. D 83 (2011) 071501. [arXiv:1009.2714](#), [doi:10.1103/PhysRevD.83.071501](#).
- [36] J. R. Gaunt, W. J. Stirling, Double Parton Scattering Singularity in One-Loop Integrals, JHEP 06 (2011) 048. [arXiv:1103.1888](#), [doi:10.1007/JHEP06\(2011\)048](#).
- [37] M. G. Ryskin, A. M. Snigirev, A Fresh look at double parton scattering, Phys. Rev. D 83 (2011) 114047. [arXiv:1103.3495](#), [doi:10.1103/PhysRevD.83.114047](#).
- [38] B. Blok, Y. Dokshitser, L. Frankfurt, M. Strikman, pQCD physics of multiparton interactions, Eur. Phys. J. C 72 (2012) 1963. [arXiv:1106.5533](#), [doi:10.1140/epjc/s10052-012-1963-8](#).
- [39] M. Diehl, D. Ostermeier, A. Schafer, Elements of a theory for multiparton interactions in QCD, JHEP 03 (2012) 089, [Erratum: JHEP 03, 001 (2016)]. [arXiv:1111.0910](#), [doi:10.1007/JHEP03\(2012\)089](#).
- [40] A. V. Manohar, W. J. Waalewijn, What is Double Parton Scattering?, Phys. Lett. B 713 (2012) 196–201. [arXiv:1202.5034](#), [doi:10.1016/j.physletb.2012.05.044](#).
- [41] M. G. Ryskin, A. M. Snigirev, Double parton scattering in double logarithm approximation of perturbative QCD, Phys. Rev. D 86 (2012) 014018. [arXiv:1203.2330](#), [doi:10.1103/PhysRevD.86.014018](#).
- [42] J. R. Gaunt, W. J. Stirling, Double Parton Distributions Incorporating Perturbative QCD Evolution and Momentum and Quark Number Sum Rules, JHEP 03 (2010) 005. [arXiv:0910.4347](#), [doi:10.1007/JHEP03\(2010\)005](#).
- [43] K. Golec-Biernat, E. Lewandowska, How to impose initial conditions for QCD evolution of double parton distributions?, Phys. Rev. D 90 (1) (2014) 014032. [arXiv:1402.4079](#), [doi:10.1103/PhysRevD.90.014032](#).
- [44] K. Golec-Biernat, E. Lewandowska, M. Serino, Z. Snyder, A. M. Stasto, Constraining the double gluon distribution by the single gluon distribution, Phys. Lett. B 750 (2015) 559–564. [arXiv:1507.08583](#), [doi:10.1016/j.physletb.2015.09.067](#).
- [45] M. Diehl, J. R. Gaunt, D. M. Lang, P. Plößl, A. Schäfer, Sum rule improved double parton distributions in position space, Eur. Phys. J. C 80 (5) (2020) 468. [arXiv:2001.10428](#), [doi:10.1140/epjc/s10052-020-8038-z](#).
- [46] M. Diehl, A. Schafer, Theoretical considerations on multiparton interactions in QCD, Phys. Lett. B 698 (2011) 389–402. [arXiv:1102.3081](#), [doi:10.1016/j.physletb.2011.03.024](#).
- [47] M. Diehl, J. R. Gaunt, P. Plößl, A. Schäfer, Two-loop splitting in double parton distributions, SciPost Phys. 7 (2) (2019) 017. [arXiv:1902.08019](#), [doi:10.21468/SciPostPhys.7.2.017](#).
- [48] H.-M. Chang, A. V. Manohar, W. J. Waalewijn, Double Parton Correlations in the Bag Model, Phys. Rev. D 87 (3) (2013) 034009. [arXiv:1211.3132](#), [doi:10.1103/PhysRevD.87.034009](#).
- [49] M. Rinaldi, S. Scopetta, V. Vento, Double parton correlations in constituent quark models, Phys. Rev. D 87 (2013) 114021. [arXiv:1302.6462](#), [doi:10.1103/PhysRevD.87.114021](#).
- [50] W. Broniowski, E. Ruiz Arriola, Valence double parton distributions of the nucleon in a simple model, Few Body Syst. 55 (2014) 381–387. [arXiv:1310.8419](#), [doi:10.1007/s00601-014-0840-4](#).
- [51] M. Rinaldi, S. Scopetta, M. Traini, V. Vento, Double parton correlations and constituent quark models: a Light Front approach to the valence sector, JHEP 12 (2014) 028. [arXiv:1409.1500](#), [doi:10.1007/JHEP12\(2014\)028](#).
- [52] W. Broniowski, E. Ruiz Arriola, K. Golec-Biernat, Generalized Valon Model for Double Parton Distributions, Few Body Syst. 57 (6) (2016) 405–410. [arXiv:1602.00254](#), [doi:10.1007/s00601-016-1087-z](#).
- [53] T. Kasemets, A. Mukherjee, Quark-gluon double parton distributions in the light-front dressed quark model, Phys. Rev. D 94 (7) (2016) 074029. [arXiv:1606.05686](#), [doi:10.1103/PhysRevD.94.074029](#).
- [54] M. Rinaldi, S. Scopetta, M. C. Traini, V. Vento, Correlations in Double Parton Distributions: Perturbative and Non-Perturbative effects, JHEP 10 (2016) 063. [arXiv:1608.02521](#), [doi:10.1007/JHEP10\(2016\)063](#).
- [55] M. Rinaldi, F. A. Ceccopieri, Relativistic effects in model calculations of double parton distribution function, Phys. Rev. D 95 (3) (2017) 034040. [arXiv:1611.04793](#), [doi:10.1103/PhysRevD.95.034040](#).
- [56] M. Rinaldi, S. Scopetta, M. Traini, V. Vento, A model calculation of double parton distribution functions of the pion, Eur. Phys. J. C 78 (9) (2018) 781. [arXiv:1806.10112](#), [doi:10.1140/epjc/s10052-018-6256-4](#).
- [57] A. Courtoy, S. Noguera, S. Scopetta, Double parton distributions in the pion in the Nambu–Jona-Lasinio model, JHEP 12 (2019) 045. [arXiv:1909.09530](#), [doi:10.1007/JHEP12\(2019\)045](#).
- [58] W. Broniowski, E. Ruiz Arriola, Double parton distribution of valence quarks in the pion in chiral quark models, Phys. Rev. D 101 (1) (2020) 014019. [arXiv:1910.03707](#), [doi:10.1103/PhysRevD.101.014019](#).
- [59] M. Rinaldi, Double parton correlations in mesons within AdS/QCD soft-wall models: a first comparison with lattice data, Eur. Phys. J. C 80 (7) (2020) 678. [arXiv:2003.09400](#), [doi:10.1140/epjc/s10052-020-8241-y](#).
- [60] A. Courtoy, S. Noguera, S. Scopetta, Two-current correlations in the pion in the Nambu and Jona-Lasinio model, Eur. Phys. J. C 80 (10) (2020) 909. [arXiv:](#)

- 2006.05300, doi:10.1140/epjc/s10052-020-08470-1.
- [61] C. Mondal, A. Mukherjee, S. Nair, Double parton distributions for a positroniumlike bound state using light-front wave functions, Phys. Rev. D 100 (9) (2019) 094002. arXiv:1906.10903, doi:10.1103/PhysRevD.100.094002.
- [62] A. M. Sirunyan, et al., Search for physics beyond the standard model in events with jets and two same-sign or at least three charged leptons in proton-proton collisions at $\sqrt{s} = 13$ TeV, Eur. Phys. J. C 80 (8) (2020) 752. arXiv:2001.10086, doi:10.1140/epjc/s10052-020-8168-3.
- [63] A. Del Fabbro, D. Treleani, A Double parton scattering background to Higgs boson production at the LHC, Phys. Rev. D 61 (2000) 077502. arXiv:hep-ph/9911358, doi:10.1103/PhysRevD.61.077502.
- [64] O. Fedkevych, A. Kulesza, Double parton scattering in four-jet production in proton-proton collisions at the LHC, Phys. Rev. D 104 (5) (2021) 054021. arXiv:2008.08347, doi:10.1103/PhysRevD.104.054021.
- [65] F. A. Ceccopieri, M. Rinaldi, Enlightening the transverse structure of the proton via double parton scattering in photon-induced interactions, Phys. Rev. D 105 (1) (2022) L011501. arXiv:2103.13480, doi:10.1103/PhysRevD.105.L011501.
- [66] B. Blok, J. Mehl, Perturbative Color Correlations in Double Parton Scattering (10 2022). arXiv:2210.13282.
- [67] K. Golec-Biernat, A. M. Stašto, Momentum sum rule and factorization of double parton distributions, Phys. Rev. D 107 (5) (2023) 054020. arXiv:2212.02289, doi:10.1103/PhysRevD.107.054020.
- [68] M. Diehl, F. Fabry, P. Ploessl, Evolution of colour correlated double parton distributions: a quantitative study (10 2023). arXiv:2310.16432.
- [69] M. Diehl, R. Nagar, P. Plößl, Quark mass effects in double parton distributions, JHEP 09 (2023) 100. arXiv:2212.07736, doi:10.1007/JHEP09(2023)100.
- [70] M. Diehl, R. Nagar, P. Ploessl, F. J. Tackmann, Evolution and interpolation of double parton distributions using Chebyshev grids, Eur. Phys. J. C 83 (6) (2023) 536. arXiv:2305.04845, doi:10.1140/epjc/s10052-023-11692-8.
- [71] G. S. Bali, M. Diehl, B. Gläßle, A. Schäfer, C. Zimmermann, Double parton distributions in the nucleon from lattice QCD, JHEP 09 (2021) 106. arXiv:2106.03451, doi:10.1007/JHEP09(2021)106.
- [72] C. Zimmermann, D. Reitinger, Double parton distributions in the nucleon on the lattice: Flavor interference effects, PoS LATTICE2022 (2023) 131. arXiv:2211.14151, doi:10.22323/1.430.0131.
- [73] J.-H. Zhang, Double Parton Distributions from Euclidean Lattice (4 2023). arXiv:2304.12481.
- [74] J. P. Vary, H. Honkanen, J. Li, P. Maris, S. J. Brodsky, A. Harindranath, G. F. de Teramond, P. Sternberg, E. G. Ng, C. Yang, Hamiltonian light-front field theory in a basis function approach, Phys. Rev. C 81 (2010) 035205. arXiv:0905.1411, doi:10.1103/PhysRevC.81.035205.
- [75] S. J. Brodsky, H.-C. Pauli, S. S. Pinsky, Quantum chromodynamics and other field theories on the light cone, Phys. Rept. 301 (1998) 299–486. arXiv:hep-ph/9705477, doi:10.1016/S0370-1573(97)00089-6.
- [76] H. Honkanen, P. Maris, J. P. Vary, S. J. Brodsky, Electron in a transverse harmonic cavity, Phys. Rev. Lett. 106 (2011) 061603. arXiv:1008.0068, doi:10.1103/PhysRevLett.106.061603.
- [77] X. Zhao, H. Honkanen, P. Maris, J. P. Vary, S. J. Brodsky, Electron g-2 in Light-Front Quantization, Phys. Lett. B 737 (2014) 65–69. arXiv:1402.4195, doi:10.1016/j.physletb.2014.08.020.
- [78] P. Wiecki, Y. Li, X. Zhao, P. Maris, J. P. Vary, Basis Light-Front Quantization Approach to Positronium, Phys. Rev. D 91 (10) (2015) 105009. arXiv:1404.6234, doi:10.1103/PhysRevD.91.105009.
- [79] D. Chakrabarti, X. Zhao, H. Honkanen, R. Manohar, P. Maris, J. P. Vary, Generalized parton distributions in a light-front nonperturbative approach, Phys. Rev. D 89 (11) (2014) 116004. arXiv:1403.0704, doi:10.1103/PhysRevD.89.116004.
- [80] Z. Hu, S. Xu, C. Mondal, X. Zhao, J. P. Vary, Transverse structure of electron in momentum space in basis light-front quantization, Phys. Rev. D 103 (3) (2021) 036005. arXiv:2010.12498, doi:10.1103/PhysRevD.103.036005.
- [81] S. Nair, C. Mondal, X. Zhao, A. Mukherjee, J. P. Vary, Basis light-front quantization approach to photon, Phys. Lett. B 827 (2022) 137005. arXiv:2201.12770, doi:10.1016/j.physletb.2022.137005.
- [82] S. Nair, C. Mondal, X. Zhao, A. Mukherjee, J. P. Vary, Massless and massive photons within basis light-front quantization, Phys. Rev. D 108 (11) (2023) 116005. arXiv:2302.13645, doi:10.1103/PhysRevD.108.116005.
- [83] S. Jia, J. P. Vary, Basis light front quantization for the charged light mesons with color singlet Nambu–Jona-Lasinio interactions, Phys. Rev. C 99 (3) (2019) 035206. arXiv:1811.08512, doi:10.1103/PhysRevC.99.035206.
- [84] J. Lan, C. Mondal, S. Jia, X. Zhao, J. P. Vary, Parton Distribution Functions from a Light Front Hamiltonian and QCD Evolution for Light Mesons, Phys. Rev. Lett. 122 (17) (2019) 172001. arXiv:1901.11430, doi:10.1103/PhysRevLett.122.172001.
- [85] J. Lan, C. Mondal, S. Jia, X. Zhao, J. P. Vary, Pion and kaon parton distribution functions from basis light front quantization and QCD evolution, Phys. Rev. D 101 (3) (2020) 034024. arXiv:1907.01509, doi:10.1103/PhysRevD.101.034024.
- [86] L. Adhikari, C. Mondal, S. Nair, S. Xu, S. Jia, X. Zhao, J. P. Vary, Generalized parton distributions and spin structures of light mesons from a light-front Hamiltonian approach, Phys. Rev. D 104 (11) (2021) 114019. arXiv:2110.05048, doi:10.1103/PhysRevD.104.114019.
- [87] J. Lan, K. Fu, C. Mondal, X. Zhao, J. P. Vary, Light mesons with one dynamical gluon on the light front, Phys. Lett. B 825 (2022) 136890. arXiv:2106.04954, doi:10.1016/j.physletb.2022.136890.
- [88] C. Mondal, S. Nair, S. Jia, X. Zhao, J. P. Vary, Pion to photon transition form factors with basis light-front quantization, Phys. Rev. D 104 (9) (2021) 094034. arXiv:2109.02279, doi:10.1103/PhysRevD.104.094034.
- [89] Y. Li, P. Maris, X. Zhao, J. P. Vary, Heavy Quarkonium in a Holographic Basis, Phys. Lett. B 758 (2016) 118–124. arXiv:1509.07212, doi:10.1016/j.physletb.2016.04.065.

- [90] Y. Li, P. Maris, J. P. Vary, Quarkonium as a relativistic bound state on the light front, Phys. Rev. D 96 (2017) 016022. [arXiv:1704.06968](#), [doi:10.1103/PhysRevD.96.016022](#).
- [91] M. Li, Y. Li, P. Maris, J. P. Vary, Radiative transitions between 0^{-+} and 1^{--} heavy quarkonia on the light front, Phys. Rev. D 98 (3) (2018) 034024. [arXiv:1803.11519](#), [doi:10.1103/PhysRevD.98.034024](#).
- [92] J. Lan, C. Mondal, M. Li, Y. Li, S. Tang, X. Zhao, J. P. Vary, Parton Distribution Functions of Heavy Mesons on the Light Front, Phys. Rev. D 102 (1) (2020) 014020. [arXiv:1911.11676](#), [doi:10.1103/PhysRevD.102.014020](#).
- [93] S. Tang, Y. Li, P. Maris, J. P. Vary, B_c mesons and their properties on the light front, Phys. Rev. D 98 (11) (2018) 114038. [arXiv:1810.05971](#), [doi:10.1103/PhysRevD.98.114038](#).
- [94] S. Tang, Y. Li, P. Maris, J. P. Vary, Heavy-light mesons on the light front, Eur. Phys. J. C 80 (6) (2020) 522. [arXiv:1912.02088](#), [doi:10.1140/epjc/s10052-020-8081-9](#).
- [95] C. Mondal, S. Xu, J. Lan, X. Zhao, Y. Li, D. Chakrabarti, J. P. Vary, Proton structure from a light-front Hamiltonian, Phys. Rev. D 102 (1) (2020) 016008. [arXiv:1911.10913](#), [doi:10.1103/PhysRevD.102.016008](#).
- [96] S. Xu, C. Mondal, J. Lan, X. Zhao, Y. Li, J. P. Vary, Nucleon structure from basis light-front quantization, Phys. Rev. D 104 (9) (2021) 094036. [arXiv:2108.03909](#), [doi:10.1103/PhysRevD.104.094036](#).
- [97] Y. Liu, S. Xu, C. Mondal, X. Zhao, J. P. Vary, Angular momentum and generalized parton distributions for the proton with basis light-front quantization, Phys. Rev. D 105 (9) (2022) 094018. [arXiv:2202.00985](#), [doi:10.1103/PhysRevD.105.094018](#).
- [98] Z. Hu, S. Xu, C. Mondal, X. Zhao, J. P. Vary, Transverse momentum structure of proton within the basis light-front quantization framework, Phys. Lett. B 833 (2022) 137360. [arXiv:2205.04714](#), [doi:10.1016/j.physletb.2022.137360](#).
- [99] T. Peng, Z. Zhu, S. Xu, X. Liu, C. Mondal, X. Zhao, J. P. Vary, Basis light-front quantization approach to Λ and Λ_c and their isospin triplet baryons, Phys. Rev. D 106 (11) (2022) 114040. [arXiv:2208.00355](#), [doi:10.1103/PhysRevD.106.114040](#).
- [100] S. Kaur, S. Xu, C. Mondal, X. Zhao, J. P. Vary, Spatial imaging of proton via leading-twist nonskewed GPDs with basis light-front quantization, Phys. Rev. D 109 (1) (2024) 014015. [arXiv:2307.09869](#), [doi:10.1103/PhysRevD.109.014015](#).
- [101] Z. Zhu, T. Peng, Z. Hu, S. Xu, C. Mondal, X. Zhao, J. P. Vary, Transverse momentum structure of strange and charmed baryons: A light-front Hamiltonian approach, Phys. Rev. D 108 (3) (2023) 036009. [arXiv:2304.05058](#), [doi:10.1103/PhysRevD.108.036009](#).
- [102] Z. Zhang, Z. Hu, S. Xu, C. Mondal, X. Zhao, J. P. Vary, Twist-3 generalized parton distribution for the proton from basis light-front quantization, Phys. Rev. D 109 (3) (2024) 034031. [arXiv:2312.00667](#), [doi:10.1103/PhysRevD.109.034031](#).
- [103] Y. Liu, S. Xu, C. Mondal, X. Zhao, J. P. Vary, Skewed generalized parton distributions of proton from basis light-front quantization (3 2024). [arXiv:2403.05922](#).
- [104] S. Kaur, J. Wu, Z. Hu, J. Lan, C. Mondal, X. Zhao, J. P. Vary, Quark and gluon distributions in ρ -meson from basis light-front quantization, Phys. Lett. B 851 (2024) 138563. [arXiv:2401.03480](#), [doi:10.1016/j.physletb.2024.138563](#).
- [105] H. Yu, Z. Hu, S. Xu, C. Mondal, X. Zhao, J. P. Vary, Transverse-momentum-dependent gluon distributions of proton within basis light-front quantization (3 2024). [arXiv:2403.06125](#).
- [106] S. Xu, C. Mondal, X. Zhao, Y. Li, J. P. Vary, Quark and gluon spin and orbital angular momentum in the proton, Phys. Rev. D 108 (9) (2023) 094002. [doi:10.1103/PhysRevD.108.094002](#).
- [107] B. Lin, S. Nair, S. Xu, Z. Hu, C. Mondal, X. Zhao, J. P. Vary, Generalized parton distributions of gluon in proton: A light-front quantization approach, Phys. Lett. B 847 (2023) 138305. [arXiv:2308.08275](#), [doi:10.1016/j.physletb.2023.138305](#).
- [108] Z. Zhu, Z. Hu, J. Lan, C. Mondal, X. Zhao, J. P. Vary, Transverse structure of the pion beyond leading twist with basis light-front quantization, Phys. Lett. B 839 (2023) 137808. [arXiv:2301.12994](#), [doi:10.1016/j.physletb.2023.137808](#).
- [109] A. Harindranath, An Introduction to light front dynamics for pedestrians, in: International School on Light-Front Quantization and Non-Perturbative QCD (To be followed by the Workshop 3-14 Jun 1996), 1996. [arXiv:hep-ph/9612244](#).
- [110] X. Zhao, A. Ilderton, P. Maris, J. P. Vary, Scattering in Time-Dependent Basis Light-Front Quantization, Phys. Rev. D 88 (2013) 065014. [arXiv:1303.3273](#), [doi:10.1103/PhysRevD.88.065014](#).
- [111] S. J. Brodsky, G. F. de Teramond, H. G. Dosch, J. Erlich, Light-Front Holographic QCD and Emerging Confinement, Phys. Rept. 584 (2015) 1–105. [arXiv:1407.8131](#), [doi:10.1016/j.physrep.2015.05.001](#).